JHEP

Published for SISSA by Springer

Received: September 8, 2015
Revised: January 14, 2016
Accepted: May 6, 2016
Published: May 16, 2016

# Enhanced charged Higgs production through $W$-Higgs fusion in $W$-$b$ scattering

**Abdesslam Arhrib,**[a,b] **Kingman Cheung,**[b,c,d] **Jae Sik Lee**[b,e] **and Chih-Ting Lu**[c]

[a] *Département de Mathématiques, Faculté des Sciences et Techniques, B.P. 416 Tangier, Morocco*

[b] *Physics Division, National Center for Theoretical Sciences, Hsinchu, Taiwan*

[c] *Department of Physics, National Tsing Hua University, Hsinchu 300, Taiwan*

[d] *Division of Quantum Phases and Devices, School of Physics, Konkuk University, Seoul 143-701, Republic of Korea*

[e] *Department of Physics, Chonnam National University, 300 Yongbong-dong, Buk-gu, Gwangju, 500-757, Republic of Korea*

*E-mail:* aarhrib@ictp.it, cheung@phys.nthu.edu.tw, jslee@jnu.ac.kr, timluyu@yahoo.com.tw

Abstract: We study the associated production of a charged Higgs boson with a bottom quark and a light quark at the LHC via $pp \to H^\pm b\, j$ in the Two Higgs Doublet Models (2HDMs). Using the effective $W$ approximation, we show that there is exact cancellation among various Feynman diagrams in high energy limit. This may imply that the production of charged Higgs can be significantly enhanced in the presence of large mass differences among the neutral Higgs bosons via $W^\pm$-Higgs fusion in the $pp \to H^\pm b\, j$ process. Particularly, we emphasize the potential enhancement due to a light pseudoscalar boson $A$, which is still allowed by the current data by which we explicitly calculate the allowed regions in $(M_A, \tan\beta)$ plane, and show that the production cross section can be as large as 0.1 pb for large $\tan\beta$. We also show that the transverse momentum distribution of the $b$ quark can potentially distinguish the $W^\pm$-$A$ fusion diagram from the top diagram. Finally, we point out further enhancement when we go beyond the 2HDMs.

Keywords: Beyond Standard Model, Higgs Physics

ArXiv ePrint: 1509.00978



doi:10.1007/JHEP05(2016)093

JHEP05(2016)093

## Contents



## 1 Introduction

A new scalar boson $h$ was discovered in the run I of LHC with $7 \oplus 8\,\text{TeV}$ energies in 2012 [1, 2]. The combined measurement of the mass of the boson performed by the ATLAS and CMS collaborations based on the data from $h \to \gamma\gamma$ and $h \to ZZ \to 4l$ channels is $m_h = 125.09 \pm 0.21\ (\text{stat.}) \pm 0.11\ (\text{syst.})\ \text{GeV}$ [3]. Furthermore, the measured properties of the new particle are best described by the standard-model (SM) Higgs boson [4, 5].

The mission of the new LHC run at 13 TeV (and later upgraded to 14 TeV) is two folds: the first task is the improvement of the scalar boson mass and scalar boson coupling measurements and the second one would be to find a clear hint of new physics. By performing accurate measurements of the scalar boson couplings to the SM particles would be helpful to determine if the Higgs-like particle is indeed the SM Higgs boson or a Higgs boson that belongs to a higher representation, such as models with extra Higgs doublets, extra triplets, or singlets. Most of higher Higgs representations with extra doublet or triplet Higgs fields predict in their spectrum one or more singly- or doubly-charged Higgs bosons. A discovery of such charged Higgs bosons would be an indisputable signal of new physics.

In the two-Higgs-doublet models (2HDMs) or the minimal supersymmetric standard model (MSSM), the charged Higgs boson can be abundantly produced both at hadron and $e^+e^-$ colliders. At hadron colliders, the charged Higgs boson can be produced through several channels:



JHEP05(2016)093

- Production from top decay. If the mass of the charged Higgs boson is smaller than $m_t - m_b$, the production of $t\bar{t}$ pairs provides an excellent source of the charged Higgs bosons. If kinematically allowed, one of the top and anti-top quarks, say the anti-top quark can decay into $H^-\bar{b}$, competing with the SM decay of $\bar{t} \to W^-\bar{b}$. This mechanism $pp \to t\bar{t} \to t\bar{b}H^-$ can provide an important source of light charged Higgs bosons and offers a much cleaner signature than that of direct production.

- Single charged Higgs production. The most important ones are $gb \to tH^-$ and $gg \to t\bar{b}H^-$ [6–10]. These are QCD processes, and thus the cross sections are expected to be large. We can also have a single charged Higgs boson produced in association with a $W^\pm$ gauge boson via the loop process $gg \to W^\pm H^\mp$ or the tree level process $b\bar{b} \to W^\pm H^\mp$ [11–15]. Similarly, the single charged Higgs boson can be produced in association with a Higgs boson: $q\bar{q}' \to W^{\pm *} \to \phi H^\pm$ where $\phi$ denotes one the the three neutral MSSM Higgs bosons [16]. Most of these processes are of the Drell-Yan type, they are expected to give substantial cross sections only for the charged Higgs mass below about 200 GeV.

- Single charged Higgs boson production associated with a bottom quark and a light quark $qb \to q'H^+b$ in the MSSM framework in which the neutral heavier Higgs bosons are almost degenerate [17].

- Charged Higgs pair production through $q\bar{q}$ annihilation [18–20] or gluon fusion.

- Resonant charged Higgs production $c\bar{s} \to H^+$, $c\bar{b} \to H^+$ [21].

At the Tevatron and LHC, detection of light charged Higgs boson with $M_{H^\pm} < m_t - m_b$ is straightforward from $t\bar{t}$ production followed by the decay $\bar{t} \to \bar{b}H^-$ or $t \to bH^+$. Such a light charged Higgs boson can be detected for any value of $\tan\beta$ in the $\tau\nu$ decay which is indeed the dominant decay mode. The ATLAS and CMS have already had an exclusion on $B(t \to bH^+) \times B(H^\pm \to \tau\nu)$ based on this decay channel [22–25].

In the MSSM and 2HDMs, the heavy charged Higgs boson with $M_{H^\pm} \gtrsim m_t$ would decay predominantly into $t\bar{b}$. The experimental search is rather difficult due to large irreducible and reducible backgrounds associated with $H^+ \to t\bar{b}$ decay. However, in refs. [26–28] it has been demonstrated that the $H^+ \to t\bar{b}$ signature can lead to a visible signal at the LHC provided that the charged Higgs mass is below 600 GeV and $\tan\beta$ is either below $\lesssim 1.5$ or above $\gtrsim 40$. An alternative decay mode to detect a heavy charged Higgs boson is $H^\pm \to \tau\nu$ [29, 30], even if such a decay is suppressed for heavy charged Higgs bosons, it has the advantage of being much cleaner than $H^+ \to t\bar{b}$. Recently, a new technique using the jet substructure for the heavy charged Higgs boson decaying to $tb$ has been proposed in [31].

In the MSSM, the branching ratio of the decay mode $B(H^\pm \to W^\pm h)$ could at best be at the level of 10% for low $\tan\beta$ while in the 2HDM-I[1] it could dominate over $B(H^+ \to t\bar{b})$. Therefore, $H^\pm \to W^\pm h$ could be an alternative channel to discover the heavy charged Higgs boson at the LHC [32, 33]. Similarly, when the CP-odd Higgs boson $A$ is light enough,

[1]See section 2 for classification of 2HDMs.



JHEP05(2016)093

the decay of $H^\pm \to W^\pm A$ could be the dominant one in the 2HDMs and could also be used to search for heavy charged Higgs bosons. Finally, in the models with higher Higgs representations such as the triplet representation of the Higgs, the charged Higgs boson could decay into $W^\pm Z$ with a significant branching fraction [34, 35]. This decay channel could lead to isolated leptons in the final state and could be used to distinguish between models with charged Higgs bosons.

The aim of this work is to study singly-charged Higgs boson production in association with a bottom quark and a jet $q'$ with the subprocess $qb \to q'H^+b$. Such a process had been studied for the first time in ref. [17] which showed that the rate is rather small in the MSSM due to a huge cancellation between the top- and Higgs-mediated diagrams as we will show. In the present study, we discuss the production rate of this process and its sensitivity to $\tan\beta$ in the 2HDMs where the masses of the heavier Higgs bosons are not fixed by one mass parameter as in the MSSM. Specifically, we demonstrate that the process possesses destructive interference between the $s$- and $t$-channel diagrams, which significantly reduces the cross section. Especially, when the two heavier neutral Higgs bosons are decoupled from the lightest one and they are degenerate, the cross section is canceled to a large extent. In addition, we show that with a relatively light CP-odd Higgs boson, which is still allowed by the current data, the production cross section of the charged Higgs boson via $W^\pm$-Higgs fusion in the $pp \to H^\pm\, b\, j$ process can be significantly enhanced at the LHC.

The organization of the work is as follows. In the next section, we write down the framework for the 2HDMs, provide analytic understanding of the process in terms of the $2 \to 2$ subprocess, and also describe the full $2 \to 3$ process in detail. We present the numerical results in section 3. Some cases beyond the 2HDMs are considered in section 4 and we conclude in section 5.

## 2 $qb \to q'H^+b$ in two Higgs doublet models

### 2.1 Brief review of two-Higgs-doublet models

In 2HDMs the electroweak symmetry breaking is performed by two scalar fields $\Phi_1$ and $\Phi_2$ which are parameterized by:[2]

$$\Phi_1 = \begin{pmatrix} \phi_1^+ \\ \frac{1}{\sqrt{2}}\left(v_1 + \phi_1^0 + i a_1\right) \end{pmatrix}; \quad \Phi_2 = \mathrm{e}^{i\xi} \begin{pmatrix} \phi_2^+ \\ \frac{1}{\sqrt{2}}\left(v_2 + \phi_2^0 + i a_2\right) \end{pmatrix}. \tag{2.1}$$

We denote $v_1 = v\cos\beta = vc_\beta$ and $v_2 = v\sin\beta = vs_\beta$. The parameterization of the general scalar potential which is gauge invariant and possesses a general CP structure can be found in [37]. In the present study we are mainly interested in Higgs coupling to fermions and gauge couplings to be listed slightly later.

The general structure for Yukawa couplings is given in the following interactions

$$-\mathcal{L}_Y = h_u\, \overline{u_R}\, Q^T\, (i\tau_2)\, \Phi_2 + h_d\, \overline{d_R}\, Q^T\, (i\tau_2)\, \left(-\eta_1^d\, \widetilde{\Phi}_1 - \eta_2^d\, \widetilde{\Phi}_2\right)$$

[2] For an overview, see ref. [36].

| | 2HDM I | 2HDM II | 2HDM III | 2HDM IV |
|---|---|---|---|---|
| $\eta_1^d$ | 0 | 1 | 0 | 1 |
| $\eta_2^d$ | 1 | 0 | 1 | 0 |
| $\eta_1^l$ | 0 | 1 | 1 | 0 |
| $\eta_2^l$ | 1 | 0 | 0 | 1 |

**Table 1**. Classification of 2HDMs satisfying the Glashow-Weinberg condition [39] which guarantees the absence of tree-level FCNC.

$$+h_l\,\overline{l_R}\,L^T\,(i\tau_2)\,\left(-\eta_1^l\,\widetilde{\Phi}_1-\eta_2^l\,\widetilde{\Phi}_2\right)\;+\;\text{h.c.} \tag{2.2}$$

where $Q^T=(u_L\,,d_L)$, $L^T=(\nu_L\,,l_L)$, and $\widetilde{\Phi}_i=i\tau_2\Phi_i^*$ with

$$i\tau_2=\begin{pmatrix}0&1\\-1&0\end{pmatrix}\,. \tag{2.3}$$

We note that there is a freedom to redefine the two linear combinations of $\Phi_2$ and $\Phi_1$ to eliminate the coupling of the up-type quarks to $\Phi_1$ [38]. The 2HDMs are classified according to the values of $\eta_{1,2}^l$ and $\eta_{1,2}^d$ as in table 1.

To define the Higgs mass eigenstates, we first rotate the imaginary components $a_i$ and the charged ones $\phi_1^+$ and $\phi_2^+$ in order to obtain the would-be-goldstones $G^0$ and $G^\pm$ that would be eaten by the longitudinal components of the $Z$ and $W^\pm$ bosons. These rotations result in an CP-odd state $a=A=-s_\beta a_1+c_\beta a_2$ and a pair of charged Higgs bosons $H^\pm=-s_\beta\phi_1^\pm+c_\beta\phi_2^\pm$. In the most general case with CP violation, the mass eigenstates of the neutral Higgs bosons are obtained by diagonalizing the $3\times3$ mass matrix $\mathcal{M}_0^2$ by an orthogonal $3\times3$ mixing matrix $O$ that relates the interaction eigenstates to the mass eigenstates as follow:

$$(\phi_1^0,\phi_2^0,a)_\alpha^T=O_{\alpha i}(H_1,H_2,H_3)_i^T \tag{2.4}$$

such that $O^T\mathcal{M}_0^2O=\text{diag}(M_{H_1}^2,M_{H_2}^2,M_{H_3}^2)$ with the ordering of $M_{H_1}\le M_{H_2}\le M_{H_3}$. Here the states $H_i$ do not have to carry any definite CP-parity and they have both CP-even and CP-odd components.

After identifying the Yukawa couplings by

$$h_u=\frac{\sqrt{2}m_u}{v}\,\frac{1}{s_\beta}\,;\quad h_d=\frac{\sqrt{2}m_d}{v}\,\frac{1}{\eta_1^d c_\beta+\eta_2^d s_\beta}\,;\quad h_l=\frac{\sqrt{2}m_l}{v}\,\frac{1}{\eta_1^l c_\beta+\eta_2^l s_\beta}\,, \tag{2.5}$$

one can easily obtain, from the above Lagrangian, the following Higgs-fermion-fermion interactions

$$\begin{aligned}-\mathcal{L}_{H_i\bar{f}f}\;=\;&\frac{m_u}{v}\left[\bar{u}\left(\frac{O_{\phi_2 i}}{s_\beta}-i\,\frac{c_\beta}{s_\beta}O_{ai}\,\gamma_5\right)u\right]H_i\\&+\frac{m_d}{v}\left[\bar{d}\left(\frac{\eta_1^dO_{\phi_1 i}+\eta_2^dO_{\phi_2 i}}{\eta_1^dc_\beta+\eta_2^ds_\beta}-i\,\frac{\eta_1^ds_\beta-\eta_2^dc_\beta}{\eta_1^dc_\beta+\eta_2^ds_\beta}O_{ai}\,\gamma_5\right)d\right]H_i\end{aligned}$$



JHEP05(2016)093

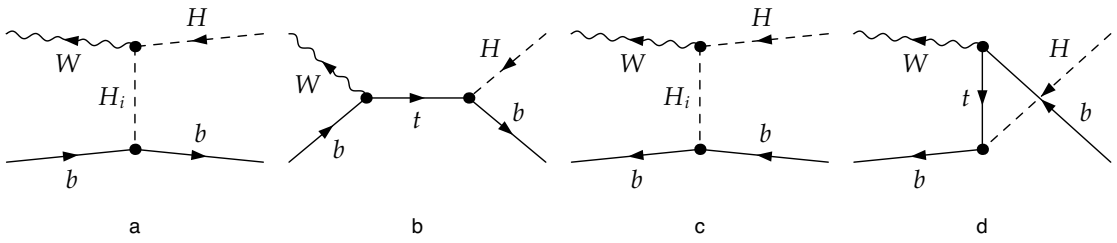


**Figure 1**. Feynman diagrams for $2 \to 2$ subprocesses: $W^+b \to H^+b$ (a) and (b), $W^+\bar{b} \to H^+\bar{b}$ (c) and (d).

$$+\frac{m_l}{v}\left[\bar{l}\left(\frac{\eta_1^l O_{\phi_1 i}+\eta_2^l O_{\phi_2 i}}{\eta_1^l c_\beta+\eta_2^l s_\beta}-i\,\frac{\eta_1^l s_\beta-\eta_2^l c_\beta}{\eta_1^l c_\beta+\eta_2^l s_\beta}O_{ai}\,\gamma_5\right)l\right]H_i \tag{2.6}$$

and

$$\begin{aligned}-\mathcal{L}_{H^\pm\bar{u}d} = &-\frac{\sqrt{2}m_u}{v}\left(\frac{c_\beta}{s_\beta}\right)\bar{u}\,P_L\,d\,H^+-\frac{\sqrt{2}m_d}{v}\left(\frac{\eta_1^d s_\beta-\eta_2^d c_\beta}{\eta_1^d c_\beta+\eta_2^d s_\beta}\right)\bar{u}\,P_R\,d\,H^+\\ &-\frac{\sqrt{2}m_l}{v}\left(\frac{\eta_1^l s_\beta-\eta_2^l c_\beta}{\eta_1^l c_\beta+\eta_2^l s_\beta}\right)\bar{\nu}\,P_R\,l\,H^+\;+\;\text{h.c.}\,,\end{aligned} \tag{2.7}$$

where $P_{L,R}=(1\mp\gamma^5)/2$.

Before moving to the next subsection, we present the mixing matrix $O$ in the CP-conserving case in terms of the mixing angle $\alpha$. In our numerical study, to deliver our findings more clearly, we focus on the CP-conserving case. In this case the matrix $O$ takes the following form:

$$O=\begin{pmatrix}-\sin\alpha & \cos\alpha & 0\\ \cos\alpha & \sin\alpha & 0\\ 0 & 0 & 1\end{pmatrix}, \tag{2.8}$$

assuming $H_3$ is the pure CP-odd state or $H_3 = A$. In this notation, the decoupling limit of the 2HDM [40], which seems to be favored by the current LHC data, is $\beta-\alpha \to \pi/2$:

$$\begin{aligned}&O_{\phi_1 1}=-\sin\alpha\to\cos\beta\,, && O_{\phi_1 2}=\cos\alpha\to\sin\beta\,;\\ &O_{\phi_2 1}=\cos\alpha\to\sin\beta\,, && O_{\phi_2 2}=\sin\alpha\to-\cos\beta\,.\end{aligned} \tag{2.9}$$

### 2.2 Subprocess $W^+ b \to H^+ b$ and unitarity

In this subsection, we present the amplitude of the process $q\,b \to q' H^\pm\,b$ in the effective $W$ approximation. In this process, the dominant contribution comes from the region where the $W$ boson emitted from the incoming quark $q$ is close to on shell and one can approximately represent the process by the $W$ boson scattering with the incoming $b$ quark or anti-$b$ quark to give $H^\pm b$ or $H^\pm\bar{b}$ in the final state:

$$\begin{aligned}&W^+(q_1)\;b(p_1)\;\to\;H^+(q_2)\;b(p_2)\,.\\ &W^+(q_1)\;\bar{b}(p_1)\;\to\;H^+(q_2)\;\bar{b}(p_2)\,.\end{aligned} \tag{2.10}$$



JHEP05(2016)093

The process $W^+b \to H^+b$ receives contributions from figure 1($a$) a $t$-channel diagram with the neutral $H_i$ exchanges and figure 1($b$) a $s$-channel diagram with top exchange. While the process $W^+\bar{b} \to H^+\bar{b}$ receives contributions from figure 1($c$) a $t$-channel diagram with the neutral $H_i$ exchanges and figure 1($d$) a $u$-channel diagram with top exchange. The relevant interactions needed for these two subprocesses can be obtained from the Yukawa interactions given by eqs. (2.6) and (2.7) and from the covariant derivatives:

$$\begin{aligned}
\mathcal{L}_{H_i\bar{b}b} &= -\frac{gm_b}{2m_W}\,\bar{b}\left(g_i^S + i\,g_i^P\,\gamma_5\right) b\,H_i\,,\\
\mathcal{L}_{H^\pm tb} &= +\frac{gm_b}{\sqrt{2}m_W}\,\bar{b}\left(c_L\,P_L + c_R\,P_R\right) t\,H^- \;+\; \text{h.c.}\,,\\
\mathcal{L}_{W^\pm tb} &= -g/\sqrt{2}\,(\bar{t}\gamma_\mu P_L\,b)\,W^{+\mu} + \text{h.c.}\,,\\
\mathcal{L}_{H_iH^\pm W^\pm} &= -\frac{g}{2}\,(S_i + iP_i)\,\left[H^-\left(i\overset{\leftrightarrow}{\partial_\mu}\right)H_i\right]\,W^{+\mu} \;+\; \text{h.c.}\,,
\end{aligned} \tag{2.11}$$

where

$$S_i = c_\beta O_{\phi_2 i} - s_\beta O_{\phi_1 i}\,, \quad P_i = O_{ai}\,, \tag{2.12}$$

and

$$c_L = \tan\beta\,, \quad c_R = \frac{m_t}{m_b}\,\frac{1}{\tan\beta}\,; \quad g_i^S = \frac{O_{\phi_1 i}}{c_\beta}\,, \quad g_i^P = -\tan\beta O_{ai} \tag{2.13}$$

in types II and IV and

$$c_L = -\frac{1}{\tan\beta}\,, \quad c_R = \frac{m_t}{m_b}\,\frac{1}{\tan\beta}\,; \quad g_i^S = \frac{O_{\phi_2 i}}{s_\beta}\,, \quad g_i^P = \frac{O_{ai}}{\tan\beta} \tag{2.14}$$

in types I and III.

The amplitude of each diagram for $W^+(q_1)\,b(p_1) \to H^+(q_2)\,b(p_2)$ reads

$$\begin{aligned}
\mathcal{M}_{(a)}^{H_i} &= -\frac{g^2 m_b}{4m_W(t-M_{H_i}^2)}\,(S_i + iP_i)\,(q_2 + p_{H_i})^\mu \epsilon_\mu(q_1)\,\left[\bar{u}(p_2)\left(g_i^S + ig_i^P\gamma_5\right)u(p_1)\right]\,,\\
\mathcal{M}_{(b)} &= -\frac{g^2 m_b C_v}{2m_W(s-m_t^2)}\left[c_L\bar{u}(p_2)\not{p}_t\not{\epsilon}(q_1)P_L u(p_1) + c_R m_t \bar{u}(p_2)\not{\epsilon}(q_1)P_L u(p_1)\right]\,,
\end{aligned} \tag{2.15}$$

where $s = (p_1+q_1)^2 = (p_2+q_2)^2$, $t = (p_1-p_2)^2 = (q_2-q_1)^2$, and $u = (p_1-q_2)^2 = (p_2-q_1)^2$ and $\epsilon^\mu(q_1)$ denotes the polarization vector of $W^+$ boson. The amplitudes for the ($c$) and ($d$) diagrams in figure 1 can be obtained by replacing $u(p_{1,2})$ with $v(p_{1,2})$ and $(s-m_t^2)$ with $(u-m_t^2)$.

In the high-energy limit, $s, |t|, |u| \gg m_W^2, m_t^2, M_{H_i}^2, M_{H^\pm}^2$, we find that

$$\begin{aligned}
\mathcal{M}_{(a)+(b)} = \sum_i \mathcal{M}_{(a)}^{H_i} + \mathcal{M}_{(b)} \approx \frac{g^2 m_b}{4m_W^2}\Bigg\{&\left[\sum_i (S_i g_i^S - P_i g_i^P) + i\sum_i (S_i g_i^P + P_i g_i^S)\right]\bar{u}(p_2)P_R u(p_1)\\
&+\left[\left(2\,c_L + \sum_i (S_i g_i^S + P_i g_i^P)\right) + i\sum_i (-S_i g_i^P + P_i g_i^S)\right]\bar{u}(p_2)P_L u(p_1)\Bigg\},
\end{aligned} \tag{2.16}$$

where we have taken the longitudinally polarized $W$ or $\epsilon^\mu(q_1) \approx q_1^\mu/m_W$: $q_1^\mu = p_t^\mu - p_1^\mu$ with $p_t^2 = s$ for the diagram ($b$) and $q_1^\mu = p_t^\mu + p_2^\mu$ with $p_t^2 = u$ for the diagram ($d$), respectively,



JHEP05(2016)093

denoting the four-momenta of the exchanging top quark with $p_t$. Incidentally, the square of the 4-momenta of the internal neutral Higgs is $p^2_{H_i} = (p_1 - p_2)^2 = t$. We note that the $c_R$ term, which is suppressed by $m_t/\sqrt{s}$, is neglected here. In types II and IV, the $c_R$ term could be important when $\tan\beta \lesssim \sqrt{m_t/m_b} \sim 7$. As shall be seen, the total cross section takes its smallest value at $\tan\beta \sim 7$. When $\tan\beta \gtrsim 7$, compared to the $c_L$ term, the $c_R$ term could be safely neglected when $\sqrt{s}/m_t \gg (m_t/m_b)/\tan^2\beta$. On the other hand, in types I and III, the $c_R$ term can be neglected only if $\sqrt{s}/m_t \gg m_t/m_b$. Therefore, the high-enegy limit should be applied with more cautions at the LHC for types I and III. But, for the 2HDM types I and III, the production cross sections are suppressed by $1/\tan^2\beta$ with increasing $\tan\beta$ and the largest value with $\tan\beta = 1$ is only $\sim 30\,\text{fb}$, as shall be shown.

The amplitude $\mathcal{M}_{(a)+(b)}$ for the $b$-initiated processes consists of the contributions from the $t$-channel Higgs-exchange diagrams $(a)$ and the $s$-channel top-exchange diagram $(b)$ . The $c_L$ term in the second line is from the $s$-channel diagram and all the others from the $t$-channel ones. Therefore, the high-energy limit has been obtained by taking $s/(s - m_t^2) \approx t/(t - M^2_{H_i}) \approx 1$. On the other hand, the high-energy limit of the amplitude $\mathcal{M}_{(c)+(d)}$ for the $\bar{b}$-initiated processes can be obtained by replacing $u(p_{1,2})$ with $v(p_{1,2})$ in eq. (2.16) and taking $u/(u - m_t^2) \approx t/(t - M^2_{H_i}) \approx 1$. We note that the high-energy behavior of $\mathcal{M}_{(a)+(b)}$ is different from that of $\mathcal{M}_{(c)+(d)}$ especially when $s$ is not large enough and there are non-negligible parts of phase space in which the high-energy limits $u/(u - m_t^2) \approx t/(t - M^2_{H_i}) \approx 1$ in $\mathcal{M}_{(c)+(d)}$ are much more difficult to achieve than the corresponding ones $s/(s - m_t^2) \approx t/(t - M^2_{H_i}) \approx 1$ in $\mathcal{M}_{(a)+(b)}$. Otherwise, the expression given by eq. (2.16) can be applicable for both the $b$- and $\bar{b}$-initiated processes.

The high-energy limit expression eq. (2.16) contains two non-interfering terms both of which grow as $\sqrt{-t}$ and therefore the absence of these unitarity-breaking terms require the following three types of sum rules:

$$\begin{aligned} 2\,c_L + \sum_i (S_i g_i^S + P_i g_i^P) &= 0\,, \\ \sum_i S_i g_i^S &= \sum_i P_i g_i^P\,, \\ \sum_i S_i g_i^P = \sum_i P_i g_i^S &= 0\,. \end{aligned} \tag{2.17}$$

The first one gives the relation between the charged Higgs coupling to $t$ and $b$ quarks $(c_L)$ and the sum over the Higgs states of the scalar and pseudoscalar products $(g_i^S S_i + g_i^P P_i)$ of the neutral Higgs couplings to $b$ quarks and those to the charged Higgs and $W$. The second relation shows the sum over the Higgs states of the scalar products should be the same as that of the pseudoscalar ones. And the third relation implies that there is no CP violation if the scalar-pseudoscalar products are summed over the three Higgs states.

These interesting sum rules can be explicitly checked in each 2HDM. In types II and IV, using the orthogonality of the mixing matrix $O$, we find that

$$\sum_i S_i g_i^S = \sum_i (O_{\phi_2 i} O_{\phi_1 i} - \tan\beta O^2_{\phi_1 i}) = -\tan\beta\,,$$



JHEP05(2016)093

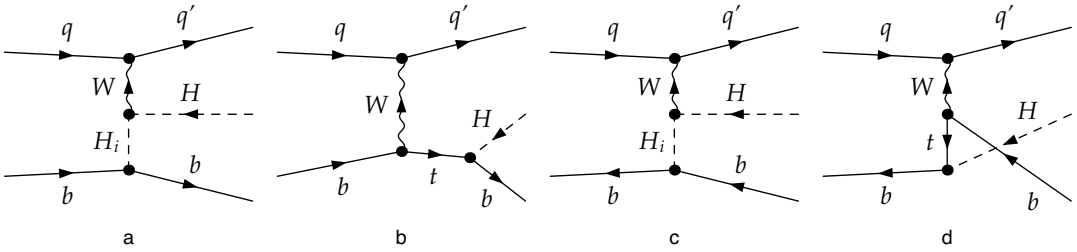


**Figure 2**. Feynman diagrams for $qb \to q'H^+b$ (a) and (b), $q\bar{b} \to q'H^+\bar{b}$ (c) and (d) where $(q, q') = (u, d), (c, s)$ and $H_i = h, H, A$. The processes with $(\bar{q}, \bar{q}') = (\bar{d}, \bar{u}), (\bar{s}, \bar{c})$ are understood.

$$\begin{aligned} \sum_i P_i g_i^P &= -\tan\beta \sum_i O_{ai}^2 = -\tan\beta\,, \\ \sum_i S_i g_i^P &= \sum_i P_i g_i^S = 0\,. \end{aligned} \tag{2.18}$$

With $c_L = \tan\beta$, the unitarity conditions are satisfied automatically. On the other hand, in types I and III, we find that

$$\begin{aligned} \sum_i S_i g_i^S &= \sum_i \left( \frac{O_{\phi_2 i}^2}{\tan\beta} - O_{\phi_1 i} O_{\phi_2 i} \right) = 1/\tan\beta\,, \\ \sum_i P_i g_i^P &= \sum_i \frac{O_{ai}^2}{\tan\beta} = 1/\tan\beta\,, \\ \sum_i S_i g_i^P &= \sum_i P_i g_i^S = 0\,. \end{aligned} \tag{2.19}$$

With $c_L = -1/\tan\beta$, the unitarity conditions are again satisfied automatically.

This is the proof for the unitarity of the subprocess $W^+b \to bH^+$ in the high energy limit in the general 2HDMs with or without CP violation. The same proof also applies to the case of $\bar{b}$ initiated subprocess $W^+\bar{b} \to \bar{b}H^+$.

### 2.3 The full process $qb \to q'H^+b$

After discussing the essence of the physics involved in the $2 \to 2$ subprocess, we shall describe the full $2 \to 3$ process.[3] We shall consider the CP-conserving case for simplicity, unless stated otherwise. In this case, without loss of generality, we identify $H_1 = h$, $H_2 = H$, and $H_3 = A$, where $h$ and $H$ denote the lighter and heavier CP-even Higgs bosons, respectively, and $A$ the CP-odd one. The Feynman diagrams for the subprocesses $qb \to q'H^+b$ and $q\bar{b} \to q'H^+\bar{b}$ are shown in figure 2. We stress at this level one important difference between the bottom-initiated diagram in figure 2(b) and anti-bottom-initiated one in figure 2(d) is that the former has a $s$-channel exchange top propagator while the latter has a $u$-channel one. Similarly, the fermion-line direction of the $q$ can be reversed to

[3]For a full consideration of NLO corrections, one may need to take account of the $2 \to 4$ process: $qg \to qH^+b\bar{b}$. We leave this part for further work.



JHEP05(2016)093

| | Type I, III | Type II, IV |
|---|---|---|
| $hb\bar{b}$ | $\frac{\cos\alpha}{\sin\beta}$ | $-\frac{\sin\alpha}{\cos\beta}$ |
| $Hb\bar{b}$ | $\frac{\sin\alpha}{\sin\beta}$ | $\frac{\cos\alpha}{\cos\beta}$ |
| $Ab\bar{b}$ | $+\cot\beta$ | $-\tan\beta$ |
| $H^-t\bar{b}$ | $-\frac{m_b}{\tan\beta}P_L+\frac{m_t}{\tan\beta}P_R$ | $m_b\tan\beta P_L+\frac{m_t}{\tan\beta}P_R$ |

**Table 2**. The bottom quark Yukawa couplings for $h, H, A$ and that of the charged Higgs boson for 2HDMs of type I, II, III, and IV. The common factor for neutral Higgs boson is $gm_b/\sqrt{2}M_W$ while that for the charged Higgs is $g/\sqrt{2}M_W$. The chiral projection operators are $P_{L,R} = (1 \mp \gamma^5)/2$.

include $\bar{q} \to \bar{q}'$ transition. Therefore, we have a number of initial states for production of $H^+$: $(u, c, \bar{d}, \bar{s}) \otimes (b, \bar{b})$. We can then take the charge conjugate to obtain the $H^-$ processes.

The diagram in figure 2(b) represents a top-induced process. If $M_{H^\pm} < m_t - m_b$, the top quark is produced on-shell, then followed by its decay into $bH^+$. This diagram is entirely dominant over the other diagrams. However, when $M_{H^\pm} > m_t - m_b$ the top quark is off-shell, and thus other diagrams also make significant contributions. In other diagrams, the charged Higgs boson appears being produced by $WH_i$ fusion, where $H_i = h, H, A$ in the CP-conserving case. The coupling in the vertex $W^+H^-H_i$ is a gauge coupling proportional to $g$ and some mixing angles of the Higgs sector, and independent of different types of 2HDMs. On the other hand, the dependence on the type of 2HDMs comes from the Yukawa couplings of $H_i$ to $b$ quark and the charged Higgs boson to $tb$. We list the relevant Yukawa couplings for 2HDMs from type I to IV in table 2 up to some normalizations. Incidentally, the non-vanishing neutral Higgs couplings to charged Higgs and $W$ are given by

$$\begin{aligned} S_1 &= S_h = c_\beta O_{\phi_2 1} - s_\beta O_{\phi_1 1} = \cos(\beta - \alpha)\,, \\ S_2 &= S_H = c_\beta O_{\phi_2 2} - s_\beta O_{\phi_1 2} = -\sin(\beta - \alpha)\,, \\ P_3 &= P_A = O_{a3} = 1\,, \end{aligned} \tag{2.20}$$

using the form of $O$ given by eq. (2.8).

In the decoupling limit, we have $\cos(\beta - \alpha) = 0$ and $\sin(\beta - \alpha) = 1$. The contribution from the light Higgs $h$ diagram is automatically zero because $S_h = 0$. The contributions from $H$ and $A$ are the same up to the $\gamma^5$ factor in the $\phi^0 b\bar{b}$ vertex if they are degenerate. If we look at the diagram more closely, the whole process can be regarded as $Wb$ and $W\bar{b}$ annihilation, as $2 \to 2$ processes. It is easy to see from figure 2 that for the $Wb \to H^+b$ subprocess we have three $t$-channel diagrams with $H_i = h, H, A$ in figure 2(a) and one $s$-channel diagram mediated by the top quark in figure 2(b). Similarly, for $W\bar{b} \to H^+\bar{b}$ subprocess we have three $t$-channel diagrams with $H_i = h, H, A$ in figure 2(c) and one $u$-channel diagram mediated by the top quark in figure 2(d). We have shown in the previous subsection using the effective $W$ approximation that there is strong cancellation among the diagrams, and indeed all four diagrams will exactly cancel one another in the high energy limit. Therefore, if we employ a much lighter CP-odd Higgs boson, which is still allowed by the current data, we expect a strong enhancement to the production cross section of this process. Experimentally, one can use this process to search for the charged Higgs boson



JHEP05(2016)093

and investigate the effects of light CP-odd Higgs boson. Perhaps, a negative search would close out the entire window of light CP-odd Higgs boson.

## 3 Numerical results

In this section, we first present some numerical results for the subprocesses $W^+b \to bH^+$ and $W^+\bar{b} \to \bar{b}H^+$ for a given value of center-of-mass energy $\sqrt{S}$ and then consider the full process $pp \to H^+bj$ in the 2HDM of type I (III) and II (IV).

### 3.1 The $2 \to 2$ subprocess in the effective $W$ approximation

We shall limit ourself to the CP conserving case taking $H_1 = h$, $H_2 = H$, and $H_3 = A$. And the couplings of the neutral Higgs bosons to the charged Higgs and $W$ are: $S_h = \cos(\beta-\alpha)$, $S_H = -\sin(\beta-\alpha)$, and $P_A = 1$. Neglecting the contribution from the lightest Higgs boson $h$ as in the decoupling limit $\cos(\beta-\alpha) \to 0$, we observe that in the high-energy limit the cross section of the subprocess behaves like

$$\sigma(W^+b \to H^+b) \propto \left|2\,c_L + S_H g_H^S + P_A g_A^P\right|^2 + \left|S_H g_H^S - P_A g_A^P\right|^2 . \tag{3.1}$$

We note that the cross section suffers a huge cancellation between the top- and Higgs-mediated diagrams and a further cancellation between the Higgs-mediated diagrams. Taking the type II model as an example, we find

$$\begin{aligned} \sigma(W^+b \to H^+b)\big|_{t\text{ only}} &\propto 4\,\tan^2\beta\,, \\ \sigma(W^+b \to H^+b)\big|_{t+H\text{ only}} &= \sigma(W^+b \to H^+b)\big|_{t+A\text{ only}} \propto 2\,\tan^2\beta\,, \\ \sigma(W^+b \to H^+b)\big|_{t+H+A} &\propto \mathcal{O}\left(\frac{m_t^2}{s} + \frac{M_{H_i}^2}{t}\right) \end{aligned} \tag{3.2}$$

with $c_L = -S_H g_H^S = -P_A g_A^P = \tan\beta$. Note, for the $W^+\bar{b} \to H^+\bar{b}$ process,

$$\sigma(W^+\bar{b} \to H^+\bar{b})\big|_{t+H+A} \propto \mathcal{O}\left(\frac{m_t^2}{u} + \frac{M_{H_i}^2}{t}\right) \tag{3.3}$$

while the high-energy behavior of the $t$-only, $(t+H)$-only, and $(t+A)$-only amplitudes remains the same.

Furthermore, independent of the type of 2HDMs we note that for $W^+b \to H^+b$ (respectively $W^+\bar{b} \to H^+\bar{b}$) the $s$-channel (respectively the $u$-channel) top-exchange diagram interferes destructively with the $t$-channel Higgs-exchange $W-A$ and $W-H$ fusion diagrams. For demonstration we show in figure 3 the cross sections for the subprocess $W^+b \to H^+b$ (left) and $W^+\bar{b} \to H^+\bar{b}$ (right) as a function of center of mass energy $\sqrt{s}$ in the MSSM.[4] We illustrate separately the top diagram alone, the sum of the top and pseudoscalar Higgs exchange diagrams, as well as all four diagrams. Note that "top+$A$" and "top+$H$" are

[4]Though we are working in the framework of 2HDMs, $M_{H^+}$, $M_H$, and $M_A$ are very close to one another in the MSSM that will suit our purpose here.

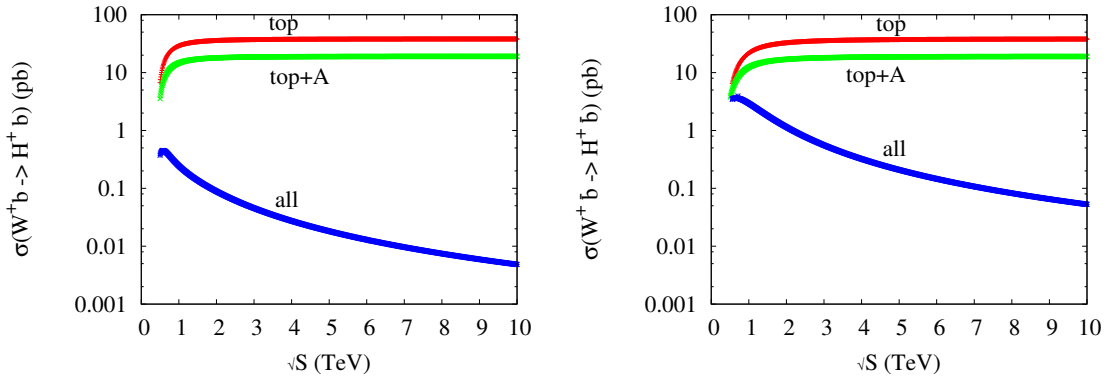


**Figure 3**. The cross section as a function of center of mass energy for the subprocess $W^+b \to H^+b$ (left) and $W^+\bar{b} \to H^+\bar{b}$ (right) in the MSSM for $\tan\beta = 30$ and $M_A = 400\,\text{GeV}$.

extremely close to each other. It is clear from the plot that the dominant contribution is coming from the top diagram. It is also visible from the plot that the interference between $s$-channel top diagram and $W$-$A$ fusion is destructive. The top contribution is reduced by a factor of 2 by the $W$-$A$ fusion diagram and same destructive interference takes place with $W$-$H$ fusion diagram. We only show the sum of the top diagram and $W$-$A$ fusion diagram in the figure, that of the top and $W$-$H$ fusion diagrams is almost the same. As expected from eq. (3.2), in the case of $W^+b \to H^+b$, after inclusion of all diagrams the total cross section drops by more than 3 orders of magnitude at large $\sqrt{s}$, as shown on the left panel of figure 3. This in fact is due to the strong destructive interference of top diagram with the $W$-$A$ and $W$-$H$ fusion diagrams. Similarly, on the right panel in figure 3 we illustrate the cross section for $W^+\bar{b} \to H^+\bar{b}$ as a function of $\sqrt{s}$. Again, as expected we can see destructive interference between $u$-channel top diagram and $t$-channel $W$-$A$ and $W$-$H$ fusion diagrams. We stress that the destructive interference in the $\bar{b}$-initiated process is less severe than the $b$-initiated one, such that the total cross section for $W^+\bar{b} \to H^+\bar{b}$ is about one order of magnitude larger than that for $W^+b \to H^+b$. This is because the cancellation between the $u$- and $t$-channel diagrams is not as effective as in the $s$- and $t$-channel diagrams. For fixed and relatively small values of $\sqrt{s}$, there are non-negligible parts of phase space in which the high-energy limits $u/(u - m_t^2) \approx 1$ and $t/(t - M_{H_i}^2) \approx 1$ can not be achieved simultaneously due to the relation $t+u = -s+M_W^2+M_{H^\pm}^2$. Therefore, the $\bar{b}$-initiated process has an order of magnitude larger cross section.

### 3.2 For full process $pp \to H^\pm bj$

In the previous subsection we have shown analytically and illustrated numerically the cancellation in the subprocesses $W^+b \to bH^+$ and $W^+\bar{b} \to H^+\bar{b}$ between the top diagram and $W$-$A$ and $W$-$H$ fusion diagrams using the effective W approximation. In figure 4, we show the cross sections for the full $2 \to 3$ processes $qb \to q'H^+b$ (upper panels), $q\bar{b} \to q'H^+\bar{b}$ (middle panels), and their sum (lower panels) as functions of $\tan\beta$ (left panels) and $M_{H^+} = M_A = M_H$ (right panels), including the charged-conjugate channels and after folding with



JHEP05(2016)093

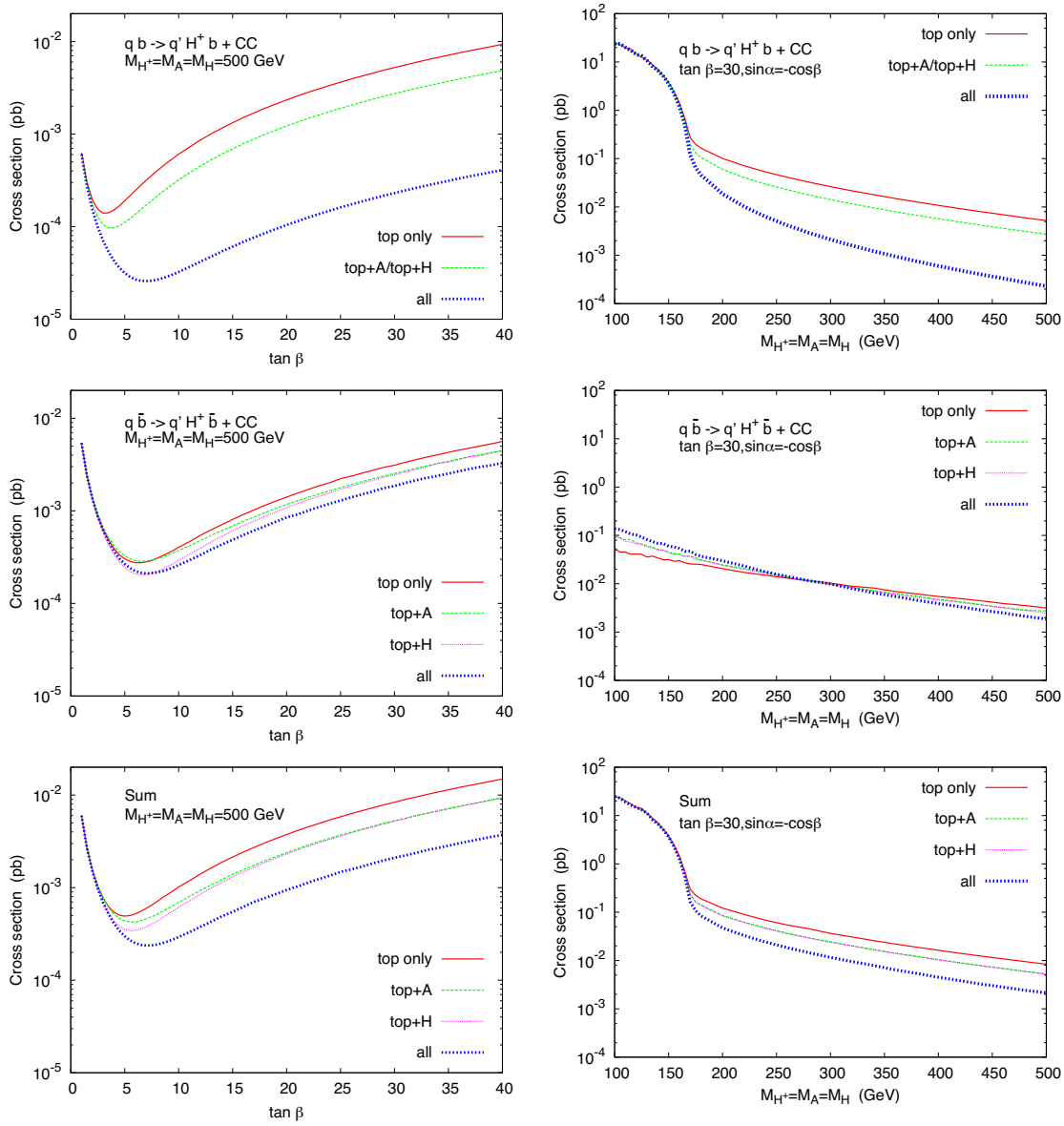


**Figure 4**. The $pp \to H^{\pm} bj$ cross sections in the 2HDM type II as functions of $\tan\beta$ (left panels) and charged Higgs mass (right panels) at LHC-14. The upper panels are the $b$ initiated process, the middle panels are $\bar{b}$ initiated process while the lower panel are the sum of $b$ and $\bar{b}$. The charged conjugate panels are included in the plots. All panels are for the decoupling limit $\sin\alpha = -\cos\beta$.

the parton distribution functions[5] Again, we separately show the contributions from the top diagram only, the top plus $W$-$A$ fusion diagrams, the top plus $W$-$H$ fusion diagrams, and all diagrams. We have assumed that we are in the decoupling limit $\sin\alpha = -\cos\beta$ and taking a spectrum of degenerate Higgs bosons $M_{H^{\pm}} = M_H = M_A$ as in the MSSM and the lightest

[5]Our numerical calculations of the several cross sections for the $b$- and $\bar{b}$-initiated full $2 \to 3$ processes presented here are carried out by use of the Helicity Amplitude Method [41]. We compare our results for the total cross sections with those obtained using `MadGraph` [42] and find excellent agreements.



JHEP05(2016)093

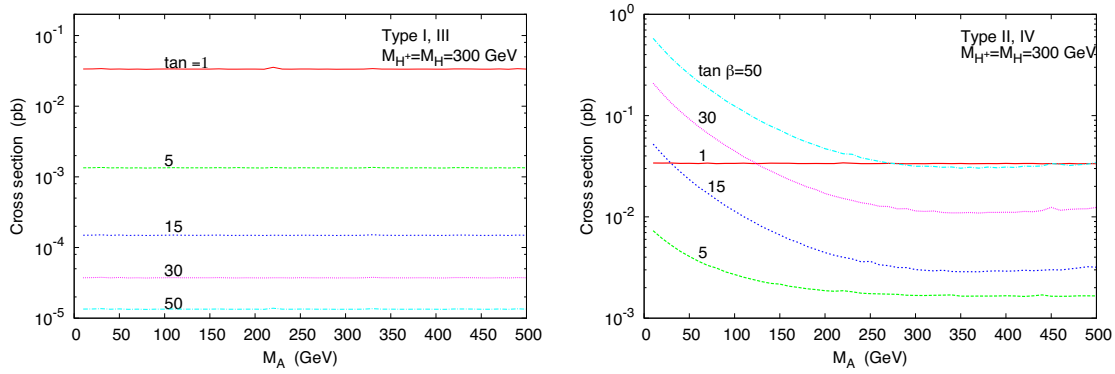


**Figure 5**. The $pp \to H^{\pm} bj$ cross sections at LHC-14 as a function of $M_A$ in the 2HDM type I and III (left), and II and IV (right) for several values of $\tan\beta$. We have taken $M_{H^{\pm}} = M_H = 300\,\text{GeV}$.

CP-even Higgs boson $h$ is the observed one with $m_h = 125.09\,\text{GeV}$. Thus, the diagram with $h$ proportional to $\cos(\beta - \alpha)$ does not contribute while the amplitudes associated with the $A$ and $H$ diagrams are the same up to a factor of $\gamma^5$ in the $Ab\bar{b}$ and $Hb\bar{b}$ vertex. Also, we can see that in the $b$-initiated subprocess (upper panels) the "top+$A$" curve completely overlaps with "top+$H$" curves but not exactly in the $\bar{b}$-initiated one (middle panels).

The upper panels in figure 4 illustrate a very strong cancellation between the top diagram, and $W$-$A$ and $W$-$H$ fusion diagrams. Note the charged-conjugate channels $\bar{q}\bar{b} \to \bar{q}' H^- \bar{b}$ are included in it. On the other hand, the middle panels show a less severe cancellation between the top diagram, and $W$-$A$ and $W$-$H$ fusion diagrams where the charged-conjugate channels $\bar{q}b \to \bar{q}' H^- b$ are also included in it. Therefore, we still see that a strong cancellation occurs for the full process $pp \to H^{\pm} bj$ at the LHC-14, shown in the lower panels. Also, note that the total cross section is dominated by the $\bar{b}$-initiated process when $M_{H^+} \gtrsim 200\,\text{GeV}$, where the internal top cannot be produced on-shell.

It is clear from the left panels that the cross sections are enhanced for both small $\tan\beta \approx 1$ and large $\tan\beta$, the latter of which is associated with enhanced bottom Yukawa couplings. A dip indeed occurs around $\tan\beta \approx 6$ in the $\tan\beta$ plots, which corresponds to where the top and bottom Yukawa couplings become similar $m_b \tan\beta \approx m_t / \tan\beta$. We stress that our results are in good agreement with ref. [17].

As shown on the right panels, we emphasize that for $M_{H^{\pm}} \leq m_t - m_b$ the top quark can be produced on-shell as in single-top production and then decays into $bH^+$, Therefore, in the range of $M_{H^{\pm}} \leq m_t - m_b$ the top-exchange diagram completely dominates over other diagrams. On the other hand, for $M_{H^{\pm}} > m_t - m_b$ the top quark is off-shell, and thus other diagrams also make significant contributions. Note that in the $\bar{b}$-initiated process $q\bar{b} \to q' H^+ \bar{b}$ the top quark is never produced on-shell.

It is well known that in the MSSM and for $M_A \geq 200\,\text{GeV}$ all the heavy Higgs bosons become degenerate $M_H = M_A = M_{H^{\pm}}$ and $\cos(\beta - \alpha) \to 0$. In general 2HDMs all Higgs boson masses are independent parameters. One can then identify the lightest CP-even with the observed 125 GeV Higgs boson and take the others $M_H$, $M_A$ and $M_{H^{\pm}}$ as free parameters. In figure 5, we show the total cross sections as a function of the CP-odd Higgs



JHEP05(2016)093

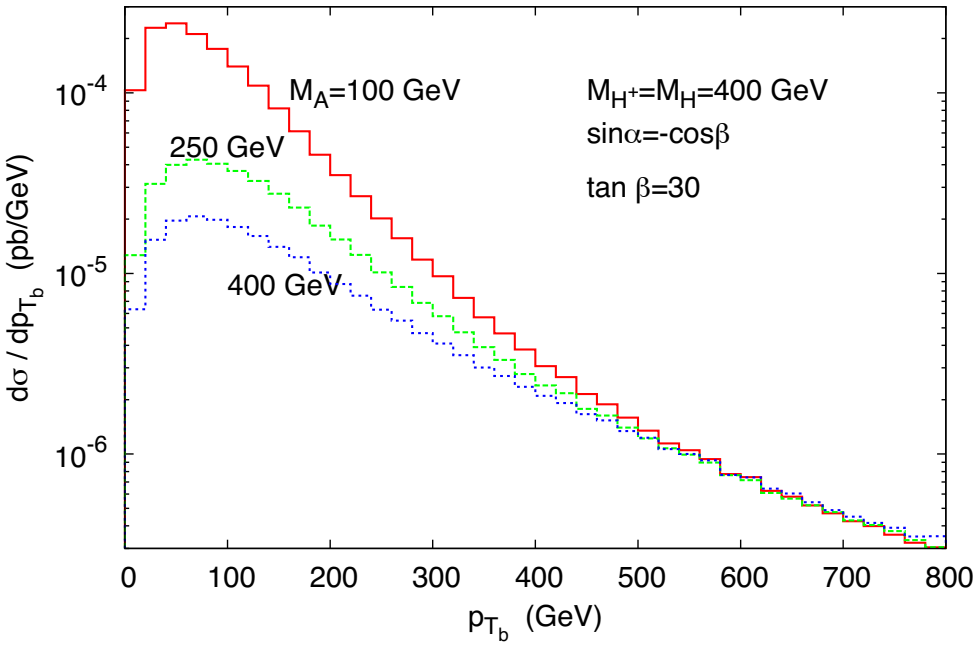


**Figure 6**. The transverse momentum $p_{T_b}$ distribution for $pp \to H^{\pm} bj$ in 2HDM type II and IV at the LHC-14 for $M_A = 100, 250, 400\,\text{GeV}$. We have taken the decoupling limit $\sin\alpha = -\cos\beta$, $\tan\beta = 30$, and $M_{H^{\pm}} = M_H = 400\,\text{GeV}$.

mass for a few values of $\tan\beta = 1 - 50$ and $M_H = M_{H^{\pm}} = 300\,\text{GeV}$ in 2HDMs types I and III (left panel) and types II and IV (right panels). Note that for this choice of masses the production cross section is dominated by the $\bar{b}$-initiated process. For the values of the couplings in production cross sections, we refer to table 2. In types I and III, the cross sections are insensitive to the CP-odd Higgs mass and they are suppressed by $1/\tan^2\beta$ with increasing $\tan\beta$. The largest value of the cross section is obtained at $\tan\beta = 1$ and is of the order 27 fb. In types II and IV, one can see some sensitivity to the CP-odd Higgs mass. For $M_A \leq 250\,\text{GeV}$, the cross section increases for lighter CP-odd Higgs mass and becomes almost constant for $M_A \geq 250\,\text{GeV}$. The enhancement of the cross section for $M_A \leq 250\,\text{GeV}$ is amplified with large values of $\tan\beta$. For $M_A = 100\,\text{GeV}$ and $\tan\beta = 30$ one can reach a cross section of the order of 40 fb.

In figure 6, we plot the $p_{T_b}$ distribution of the $b$ quark in the decoupling limit and for $M_{H^{\pm}} = M_H = 400\,\text{GeV}$ and $\tan\beta = 30$ for several values of $M_A = 100, 250$ and $400\,\text{GeV}$. As one can see from the plot, the distribution is enhanced for light $M_A = 100\,\text{GeV}$ and for $p_{T_b} \leq 200\,\text{GeV}$. The transverse momentum of the $b$ quark is then a useful variable to separate the contributions between the top diagram and the $W$-$A$ fusion diagram. One can require $p_{T_b} < 200\,\text{GeV}$ to suppress the top-exchange contribution. Therefore, we can see that the $W$-$A$ fusion diagram dominates for light $M_A$ and at the lower $p_{T_b}$ region.



JHEP05(2016)093

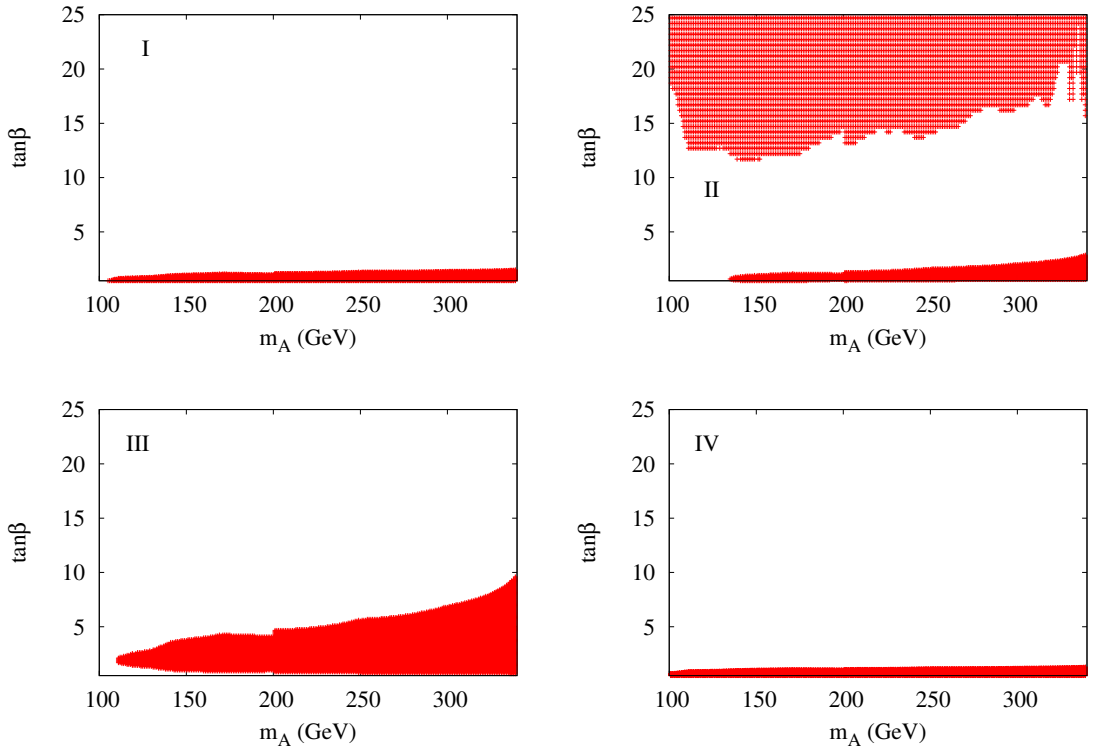


**Figure 7**. Exclusion plots in the plane of $(M_A, \tan\beta)$ for the 2HDMs type I, II, III and IV, using the ATLAS data for $gg \to A \to \tau^+\tau^-$. The excluded region is shown in red while the rest is allowed.

### 3.3 Large $\tan\beta$ and LHC $pp \to \Phi \to \tau^+\tau^-$ data

At the LHC with 7 and 8 TeV, searches for the Higgs bosons $\Phi$ that decay into tau pairs, which in turn decay into those final states with one or two light leptons, have been performed [43, 44] for Higgs mass in the range $[100, 900]$ GeV. Both ATLAS and CMS have some exclusion limits given as $\sigma(gg \to \Phi) \times B(\Phi \to \tau^+\tau^-)$ as a function of the Higgs mass $m_\Phi$. These limits can be interpreted in the 2HDMs if we take the Higgs state $\Phi$ as one of the neutral Higgs bosons of the 2HDMs: $\Phi = h$ and/or $H, A$. In fact if $h$ mimics the SM Higgs boson, $\sigma(gg \to h) \times B(h \to \tau^+\tau^-)$ will not have any enhancement factor such as $\tan\beta$. Since we have observed that in order to enhance $pp \to bH^+j$ cross sections one needs both non-degenerate $A$ and $H$ and also large $\tan\beta$, here we attempt to find what would be the largest possible value for $\tan\beta$ such that it is still consistent with $\tau^+\tau^-$ data for $100 \le M_A \le 340$ GeV and assuming that the heavy CP-even Higgs boson is rather heavy. A similar study with the 7 TeV data had been done in [45] for 2HDM. Because of CP invariance the CP-odd Higgs boson $A$ does not couple to $WW$ or $ZZ$, and the partial decay widths into loop mediated $gg$, $\gamma\gamma$, and $\gamma Z$ channels are highly suppressed. The decay channel $A \to hZ$, which is proportional to $\cos(\beta - \alpha)$, will also be severely suppressed if we assume that $\beta - \alpha$ is close to the decoupling limit. Therefore, the CP-odd Higgs boson predominantly decays into fermion pairs: $q\bar{q}$, $q = b, s, d, c, u$ and $l^+l^-$ $l = \tau, \mu, e$.



JHEP05(2016)093

In 2HDM-I and -IV, the coupling $A\tau^+\tau^-$ is proportional to $1/\tan\beta$ while in 2HDM-II and -III it is proportional to $\tan\beta$. On the other hand, from table 1 the coupling of $Ab\bar{b}$ is proportional to $\tan\beta$ in 2HDM-II and -IV but $1/\tan\beta$ in 2HDM-I and -III. Thus, it is clear that in 2HDM-I (resp. II) both the production rate $gg \to A$ and the decay $A \to \tau^+\tau^-$ are suppressed (resp. enhanced) for large $\tan\beta$. We then expect a strong exclusion for large $\tan\beta$ in type II but not in type I. In all four 2HDM types we expect some enhancement for small $0.5 \leq \tan\beta \leq 1$ because $At\bar{t}$ is proportional to $m_t/\tan\beta$.

For a given CP-odd Higgs mass $M_A$ and $\tan\beta$, the cross section of $gg \to A$, which only depends on these 2 parameters, is computed with help of SUSHI public code [46]. In the decoupling limit $A \to Zh$ is vanishing, and if $A \to \{W^\pm H^\mp, ZH, t\bar{t}\}$ are closed, the branching ratio of $A \to \tau^+\tau$ depends on $\tan\beta$ and $M_A$ only, and there is no $\sin\alpha$ dependence. Therefore, the cross section $gg \to A \to \tau^+\tau^-$ will depend only on $\tan\beta$ and $M_A$. Hence, our exclusion from $\tau^+\tau^-$ data can be given in the plane of $(M_A, \tan\beta)$. After computing the cross section $gg \to A$ times the branching fraction of $A \to \tau^+\tau^-$, we compare our theoretical predictions with the ATLAS data [43]. Note that the ATLAS data were given for $M_A = 90, 100, \ldots 340\,\text{GeV}$ with steps of 10 GeV or even larger in some cases. Therefore, we have used linear interpolations for $M_A$ values in-between the data.

We draw in figure 7 the exclusion region in $(M_A, \tan\beta)$ plane for 2HDMs type I, II, III, and IV, where $M_A$ is in the range $[100, 340]\,\text{GeV}$ and $0.5 \leq \tan\beta \leq 50$. In 2HDM types I and IV, there is no exclusion for $\tan\beta \geq 1.5$. The reason is that in type I, the production rate of $gg \to A$ and decay of $A \to \tau^+\tau^-$ are both suppressed by $1/\tan\beta$. Whereas in 2HDM type IV, the production rate is enhanced by the bottom Yukawa for large $\tan\beta$ but the decay $A \to \tau^+\tau^-$ is suppressed by $1/\tan\beta$ which cancels the bottom enhancement in the production, which then gives no exclusion for large $\tan\beta$. In 2HDM type III, similar to type I the production rate is suppressed by $1/\tan\beta$. However, the branching fractions of $A \to q\bar{q}$ are suppressed by $1/\tan\beta$ while $B(A \to \tau^+\tau^+)$ is enhanced for large $\tan\beta$. For this reason the exclusion in type III is somewhat stronger than that in type I. There is no exclusion for $\tan\beta \geq 9.5$ (resp. $\tan\beta \geq 2$) for $M_A \approx 340\,\text{GeV}$ (resp. for $M_A \approx 112\,\text{GeV}$). On the other hand, the 2HDM-II receives both enhancement at large $\tan\beta$ for the production rate $gg \to A$ and the $B(A \to \tau^+\tau^-)$. Thus, this gives a strong exclusion for $\tan\beta \geq 22$ for all $M_A \in [100, 340]\,\text{GeV}$. The low $\tan\beta \leq 3$ region (resp. $\tan\beta \leq 1$) is also excluded for $M_A = 340\,\text{GeV}$ (resp. $M_A = 150\,\text{GeV}$).

## 4 Beyond two-Higgs-doublet models

Another interesting possibility to enhance the production of charged Higgs boson might be the case in which a 2HDM is not an ultraviolet (UV) complete theory and the UV cutoff locates far above the mass scale of heavy Higgs bosons.[6] In this case, taking one of the 2HDMs as a low-energy reference model, the relevant interactions may be parameterized as

$$\mathcal{L}_{H_i\bar{b}b} = -\frac{g m_b}{2 m_W}\,\bar{b}\left(\xi_i^S\, g_i^S + i\,\xi_i^P\, g_i^P\,\gamma_5\right) b\, H_i\,,$$

[6] We note that this kind of enhancement arising from unitarity violation might be dangerous and should be taken with caution, because a UV-complete model might contain new interactions to restore the unitarity.



JHEP05(2016)093

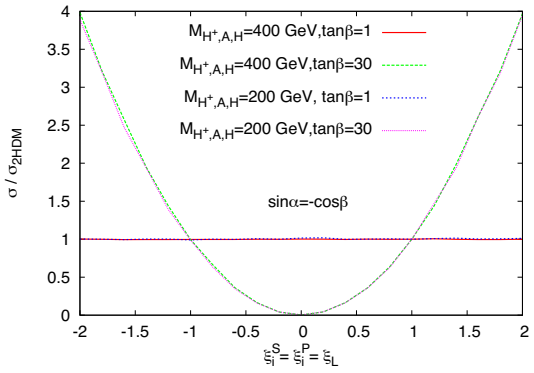


**Figure 8**. Ratios of cross sections for varying $\xi_i^S = \xi_i^P = \xi_L$ to the cross section at the 2HDM type II value ($\xi_i^S = \xi_i^P = \xi_L = 1$), showing the enhancement due to the modification of the 2HDM as suggested in the text.

$$\mathcal{L}_{H^\pm tb} = +\frac{g m_b}{\sqrt{2} m_W}\,\bar{b}\,(\xi_L\, c_L\, P_L + \xi_R\, c_R\, P_R)\, t\, H^- \;+\; \text{h.c.}\,,$$
$$\mathcal{L}_{H_i H^\pm W^\pm} = -\frac{g}{2}\,(\xi_S\, S_i + i\xi_P\, P_i)\,\left[H^-\left(i\overleftrightarrow{\partial_\mu}\right) H_i\right]\, W^{+\mu} \;+\; \text{h.c.}\,. \tag{4.1}$$

In the MSSM, for example, including the $\tan\beta$-enhanced SUSY threshold corrections to the down-type Yukawa couplings, we have

$$\xi_i^S = \xi_i^P = \xi_L = \frac{1}{1+\kappa_b \tan\beta}\,, \quad \xi_R = \xi_S = \xi_P = 1\,, \tag{4.2}$$

with [47]

$$\kappa_b = \epsilon_g + \epsilon_H,$$

where $\epsilon_g$ and $\epsilon_H$ are the contributions from the sbottom-gluino exchange diagram and from stop-Higgsino diagram, respectively. Their explicit expressions are

$$\epsilon_g = \frac{2\alpha_s}{3\pi} M_3^* \mu^* I(m^2_{\tilde{b}_1}, m^2_{\tilde{b}_2}, |M_3|^2), \qquad \epsilon_H = \frac{|h_t|^2}{16\pi^2} A_t^* \mu^* I(m^2_{\tilde{t}_1}, m^2_{\tilde{t}_2}, |\mu|^2)\,,$$

where $M_3$ is the gluino mass parameter, $h_t$ and $A_t$ are the top-quark Yukawa and trilinear couplings, respectively.

Without loss of generality we choose the 2HDM type II as the reference model, and show the change in production cross sections with the variations in the couplings $\xi_i^{S,P}$ and $\xi_L$. We used eq. (4.2) as the guidance. We first show the ratio of the cross sections for varying $\xi_i^S = \xi_i^P = \xi_L$ between $-2$ and $+2$ to the cross section at the 2HDM type II values, i.e., $\xi_i^S = \xi_i^P = \xi_L = 1$ in figure 8, for $\tan\beta = 1, 30$. The $\tan\beta = 1$ curves show almost no sensitivity to $\xi_i^S = \xi_i^P = \xi_L$ because the process is dominated by the top-Yukawa term. On the other hand, the $\tan\beta = 30$ curves are dominated by the bottom-Yukawa term. It is obvious that the ratio is close to zero for $\xi_i^S = \xi_i^P = \xi_L = 0$, and is one for $\xi_i^S = \xi_i^P = \xi_L = 1$. The ratio grows as the square of the couplings around 0 to almost 4 at $\xi_i^S = \xi_i^P = \xi_L = \pm 2$.

If for some higher scale dynamics such that $\xi_i^S$ and $\xi_i^P$ do not change in the same manner, we show the effects on the cross sections in figure 9. On the left panel, we show



JHEP05(2016)093

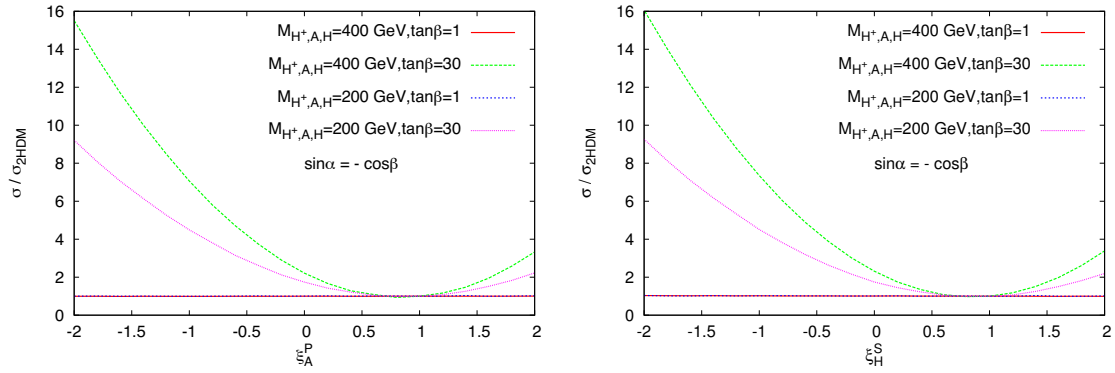


**Figure 9**. Ratios of cross section with varying $\xi_A^P$ (left panel) or $\xi_H^S$ (right panel) to the cross section at the 2HDM value (i.e. $\xi_A^P = 1$ or $\xi_H^S = 1$ respectively) by keeping all other parameters at their 2HDM type II values.

the ratio of cross sections with varying $\xi_A^P$ between $-2$ and $+2$ to the cross section at the 2HDM value (i.e. $\xi_A^P = 1$) by keeping all other parameters at their 2HDM type II values. Again, the sensitivity at $\tan\beta = 1$ is negligible, while it becomes quite nontrivial for large $\tan\beta = 30$. As we have shown in section III that the $W$-$A$ diagram interferes destructively with the top diagram, we can now turn the destructive interference into constructive one by reversing the sign of $\xi_A^P$. Furthermore, when $\xi_A^P$ is negative the second term in eq. (3.1) would not vanish. It is then very clear that the ratio becomes quite large at negative $\xi_A^P$. At $\xi_A^P = 0$, the ratio is already larger than 1 because no interference comes from the $W$-$A$ diagram. Similar behavior occurs for $\xi_H^S$ as shown on the right panel in figure 9. The ratios that $\xi_H^S$ can attain are very similar to those of $\xi_A^P$.

## 5 Conclusions

We have performed the study of $b$- and $\bar{b}$-initiated processes of $pp \to jH^\pm b/\bar{b}$ in the 2HDM framework at the LHC-14 in the decoupling limit ($\sin\alpha = -\cos\beta$), which is favored by the current Higgs data. We have identified strong cancellations between the top diagram and the $W$-$H_i (H_i = h, H, A)$ diagrams which rendered the process very suppressed. The cancellation is indeed the strongest when the $A$ and $H$ are degenerate and in the decoupling limit. We pointed out that if the pseudoscalar Higgs boson $A$ is much lighter than the CP-even Higgs boson $H$, the cross section of charged-Higgs production can be substantially enhanced, because the cancellation is no longer complete. We have explicitly obtained the exclusion in parameter space of $(M_A, \tan\beta)$ for 2HDM types I to IV based on the LHC data on $\sigma(g \to \Phi) \times B(\Phi \to \tau^+\tau^-)$. In the allowed paramete space, the size of production cross section can be as large as $\mathcal{O}(50)\,\text{fb}$ for $M_A = 100\,\text{GeV}$ and $\tan\beta = 30$ for types II and IV. This is the main result of the work.

We offer the following comments on the findings of this work as follows.

1. The $b$-initiated process for production of $H^+$ in $qb \to qH^+b$ suffers from a very strong cancellation between the top diagram and the $W$-$H_i$ diagrams. However,



JHEP05(2016)093

the $\bar{b}$-initiated process for production of $H^+$ in $q\bar{b} \to qH^+\bar{b}$ suffers a less severe cancellation, mainly because of the $u$-channel top-exchange instead of $s$-channel.

2. The strong cancellation is dictated by the absence of the unitarity-breaking terms and we find the sum rules expressed by the relevant Higgs couplings, see eq. (2.17).

3. For $M_{H^\pm} \leq m_t - m_b$ the top diagram completely dominates as the top quark is produced on-shell as like that in single-top production. However, when $M_{H^\pm} > m_t - m_b$ the $W$-$H_i$ fusion diagrams also contribute.

4. In the future study, we shall make use of the special kinematics, e.g, the $p_{T_b}$ distribution, to discriminate between the top and the $W$-$H_i$ fusion diagrams. The goal is to isolate the effect of light pseudoscalar Higgs boson, which is still allowed by the current data.

5. Current LHC data on $\sigma(gg \to \Phi) \times B(\Phi \to \tau^+\tau^-)$ constrains the parameters of the 2HDMs. We found that the data constrains the most on type II because both the production process and the decay are $\tan\beta$ enhanced. Yet, there are sizable allowed parameter space between $\tan\beta = 3$ and 22. The second most constrained is type III because the production rate is suppressed by $1/\tan\beta$ but the decay is enhanced by $\tan\beta$. Types I and IV have the most available parameter space.

6. The process $pp \to jH^\pm b/\bar{b}$ that we consider in this work would be more interesting for type II and IV because of larger cross sections. Especially type IV has the least restriction from the current LHC data on $\sigma(gg \to \Phi) \times B(\Phi \to \tau^+\tau^-)$, and it can allow cross sections as large as $O(100-300)$ fb for $\tan\beta = 30-50$ and $M_A = 50-100$ GeV.

7. When the 2HDM is a low-energy limit of some ultraviolet (UV) models, the integrity of the Yukawa couplings may change. For example, in the MSSM the SUSY particles can largely change the bottom-Yukawa couplings with strong and weak interactions. Varying the bottom Yukawa coupling of either $A$ or $H$ gives non-trivial behavior for the production cross sections.

## Acknowledgments

We thanks Marco O. P Sampaio for providing us with CP-odd cross sections. K.C. was supported by the MoST of Taiwan under Grants number 102-2112-M-007-015-MY3. J.S.L. was supported by the National Research Foundation of Korea (NRF) grant (No. 2013R1A2A2A01015406). A.A would like to thank NCTS for warm hospitality where part of this work has been done.





JHEP05(2016)093

## References


[1] ATLAS collaboration, *Observation of a new particle in the search for the standard model Higgs boson with the ATLAS detector at the LHC*, *Phys. Lett.* **B 716** (2012) 1 [arXiv:1207.7214] [INSPIRE].

[2] CMS collaboration, *Observation of a new boson at a mass of* 125 *GeV with the CMS experiment at the LHC*, *Phys. Lett.* **B 716** (2012) 30 [arXiv:1207.7235] [INSPIRE].

[3] ATLAS and CMS collaborations, *Combined measurement of the Higgs boson mass in pp collisions at* $\sqrt{s} = 7$ *and* 8 *TeV with the ATLAS and CMS experiments*, *Phys. Rev. Lett.* **114** (2015) 191803 [arXiv:1503.07589] [INSPIRE].

[4] K. Cheung, J.S. Lee and P.-Y. Tseng, *Higgs precision (Higgcision) era begins*, *JHEP* **05** (2013) 134 [arXiv:1302.3794] [INSPIRE].

[5] K. Cheung, J.S. Lee and P.-Y. Tseng, *Higgs precision analysis updates* 2014, *Phys. Rev.* **D 90** (2014) 095009 [arXiv:1407.8236] [INSPIRE].

[6] V.D. Barger, R.J.N. Phillips and D.P. Roy, *Heavy charged Higgs signals at the LHC*, *Phys. Lett.* **B 324** (1994) 236 [hep-ph/9311372] [INSPIRE].

[7] J.F. Gunion, H.E. Haber, F.E. Paige, W.-K. Tung and S.S.D. Willenbrock, *Neutral and charged Higgs detection: heavy quark fusion, top quark mass dependence and rare decays*, *Nucl. Phys.* **B 294** (1987) 621 [INSPIRE].

[8] R.M. Barnett, H.E. Haber and D.E. Soper, *Ultraheavy particle production from heavy partons at hadron colliders*, *Nucl. Phys.* **B 306** (1988) 697 [INSPIRE].

[9] J.L. Diaz-Cruz and O.A. Sampayo, *Contribution of gluon fusion to the production of charged Higgs at hadron colliders*, *Phys. Rev.* **D 50** (1994) 6820 [INSPIRE].

[10] F. Borzumati, J.-L. Kneur and N. Polonsky, *Higgs-strahlung and R-parity violating slepton-strahlung at hadron colliders*, *Phys. Rev.* **D 60** (1999) 115011 [hep-ph/9905443] [INSPIRE].

[11] D.A. Dicus, J.L. Hewett, C. Kao and T.G. Rizzo, $W^{\pm}H^{\mp}$ *production at hadron colliders*, *Phys. Rev.* **D 40** (1989) 787 [INSPIRE].

[12] A.A. Barrientos Bendezu and B.A. Kniehl, $W^{\pm}H^{\mp}$ *associated production at the Large Hadron Collider*, *Phys. Rev.* **D 59** (1999) 015009 [hep-ph/9807480] [INSPIRE].

[13] A.A. Barrientos Bendezu and B.A. Kniehl, *Squark loop correction to* $W^{\pm}H^{\mp}$ *associated hadroproduction*, *Phys. Rev.* **D 63** (2001) 015009 [hep-ph/0007336] [INSPIRE].

[14] W. Hollik and S.-H. Zhu, $O(\alpha_s)$ *corrections to* $b\bar{b} \to W^{\pm}H^{\mp}$ *at the CERN Large Hadron Collider*, *Phys. Rev.* **D 65** (2002) 075015 [hep-ph/0109103] [INSPIRE].

[15] O. Brein, W. Hollik and S. Kanemura, *The MSSM prediction for* $W^{\pm}H^{\mp}$ *production by gluon fusion*, *Phys. Rev.* **D 63** (2001) 095001 [hep-ph/0008308] [INSPIRE].

[16] Q.-H. Cao, S. Kanemura and C.P. Yuan, *Associated production of CP odd and charged Higgs bosons at hadron colliders*, *Phys. Rev.* **D 69** (2004) 075008 [hep-ph/0311083] [INSPIRE].

[17] S. Moretti and K. Odagiri, *Production of charged Higgs bosons of the minimal supersymmetric standard model in b quark initiated processes at the large hadron collider*, *Phys. Rev.* **D 55** (1997) 5627 [hep-ph/9611374] [INSPIRE].


JHEP05(2016)093

[18] A.C. Bawa, C.S. Kim and A.D. Martin, *Charged Higgs production at hadron colliders*, *Z. Phys.* **C 47** (1990) 75 [INSPIRE].

[19] A.A. Barrientos Bendezu and B.A. Kniehl, *$H^+H^-$ pair production at the Large Hadron Collider*, *Nucl. Phys.* **B 568** (2000) 305 [hep-ph/9908385] [INSPIRE].

[20] A. Krause, T. Plehn, M. Spira and P.M. Zerwas, *Production of charged Higgs boson pairs in gluon-gluon collisions*, *Nucl. Phys.* **B 519** (1998) 85 [hep-ph/9707430] [INSPIRE].

[21] S. Dittmaier, G. Hiller, T. Plehn and M. Spannowsky, *Charged-Higgs collider signals with or without flavor*, *Phys. Rev.* **D 77** (2008) 115001 [arXiv:0708.0940] [INSPIRE].

[22] ATLAS collaboration, *Search for charged Higgs bosons decaying via $H^\pm \to \tau^\pm\nu$ in fully hadronic final states using pp collision data at $\sqrt{s} = 8$ TeV with the ATLAS detector*, *JHEP* **03** (2015) 088 [arXiv:1412.6663] [INSPIRE].

[23] CMS collaboration, *Search for a charged Higgs boson in pp collisions at $\sqrt{s} = 8$ TeV*, *JHEP* **11** (2015) 018 [arXiv:1508.07774] [INSPIRE].

[24] CMS collaboration, *Search for a light charged Higgs boson in top quark decays in pp collisions at $\sqrt{s} = 7$ TeV*, *JHEP* **07** (2012) 143 [arXiv:1205.5736] [INSPIRE].

[25] CMS collaboration, *Search for charged Higgs bosons with the $H^+ \to \tau\nu$ decay channel in the fully hadronic final state at $\sqrt{s} = 8$ TeV*, CMS-PAS-HIG-14-020, CERN, Geneva Switzerland (2014).

[26] V.D. Barger, R.J.N. Phillips and D.P. Roy, *Heavy charged Higgs signals at the LHC*, *Phys. Lett.* **B 324** (1994) 236 [hep-ph/9311372] [INSPIRE].

[27] D.J. Miller, S. Moretti, D.P. Roy and W.J. Stirling, *Detecting heavy charged Higgs bosons at the CERN LHC with four b quark tags*, *Phys. Rev.* **D 61** (2000) 055011 [hep-ph/9906230] [INSPIRE].

[28] S. Moretti and D.P. Roy, *Detecting heavy charged Higgs bosons at the LHC with triple b tagging*, *Phys. Lett.* **B 470** (1999) 209 [hep-ph/9909435] [INSPIRE].

[29] K. Odagiri, *Searching for heavy charged Higgs bosons in the $\tau$-neutrino decay mode at LHC*, hep-ph/9901432 [INSPIRE].

[30] S. Raychaudhuri and D.P. Roy, *Sharpening up the charged Higgs boson signature using $\tau$ polarization at LHC*, *Phys. Rev.* **D 53** (1996) 4902 [hep-ph/9507388] [INSPIRE].

[31] S. Yang and Q.-S. Yan, *Searching for heavy charged Higgs boson with jet substructure at the LHC*, *JHEP* **02** (2012) 074 [arXiv:1111.4530] [INSPIRE].

[32] M. Drees, M. Guchait and D.P. Roy, *Signature of charged to neutral Higgs boson decay at the LHC in SUSY models*, *Phys. Lett.* **B 471** (1999) 39 [hep-ph/9909266] [INSPIRE].

[33] S. Moretti, *The $W^\pm h$ decay channel as a probe of charged Higgs boson production at the Large Hadron Collider*, *Phys. Lett.* **B 481** (2000) 49 [hep-ph/0003178] [INSPIRE].

[34] K. Cheung and D.K. Ghosh, *Triplet Higgs boson at hadron colliders*, *JHEP* **11** (2002) 048 [hep-ph/0208254] [INSPIRE].

[35] C.-W. Chiang and K. Tsumura, *Properties and searches of the exotic neutral Higgs bosons in the Georgi-Machacek model*, *JHEP* **04** (2015) 113 [arXiv:1501.04257] [INSPIRE].

[36] G.C. Branco, P.M. Ferreira, L. Lavoura, M.N. Rebelo, M. Sher and J.P. Silva, *Theory and phenomenology of two-Higgs-doublet models*, *Phys. Rept.* **516** (2012) 1 [arXiv:1106.0034] [INSPIRE].

JHEP05(2016)093

[37] K. Cheung, J.S. Lee and P.-Y. Tseng, *Higgcision in the two-Higgs doublet models*, *JHEP* **01** (2014) 085 [arXiv:1310.3937] [INSPIRE].

[38] S. Davidson and H.E. Haber, *Basis-independent methods for the two-Higgs-doublet model*, *Phys. Rev.* **D 72** (2005) 035004 [*Erratum ibid.* **D 72** (2005) 099902] [hep-ph/0504050] [INSPIRE].

[39] S.L. Glashow and S. Weinberg, *Natural conservation laws for neutral currents*, *Phys. Rev.* **D 15** (1977) 1958 [INSPIRE].

[40] J.F. Gunion and H.E. Haber, *The CP conserving two Higgs doublet model: the approach to the decoupling limit*, *Phys. Rev.* **D 67** (2003) 075019 [hep-ph/0207010] [INSPIRE].

[41] V.D. Barger, A.L. Stange and R.J.N. Phillips, *Four heavy quark hadroproduction*, *Phys. Rev.* **D 44** (1991) 1987 [INSPIRE].

[42] J. Alwall et al., *The automated computation of tree-level and next-to-leading order differential cross sections and their matching to parton shower simulations*, *JHEP* **07** (2014) 079 [arXiv:1405.0301] [INSPIRE].

[43] ATLAS collaboration, *Search for neutral Higgs bosons of the minimal supersymmetric standard model in pp collisions at* $\sqrt{s} = 8$ *TeV with the ATLAS detector*, *JHEP* **11** (2014) 056 [arXiv:1409.6064] [INSPIRE].

[44] CMS collaboration, *Higgs to* $\tau\tau$ *(MSSM)*, CMS-PAS-HIG-13-021, CERN, Geneva Switzerland (2013).

[45] A. Arhrib, C.-W. Chiang, D.K. Ghosh and R. Santos, *Two Higgs doublet model in light of the standard model* $H \to \tau^+\tau^-$ *search at the LHC*, *Phys. Rev.* **D 85** (2012) 115003 [arXiv:1112.5527] [INSPIRE].

[46] R.V. Harlander, S. Liebler and H. Mantler, *SusHi: a program for the calculation of Higgs production in gluon fusion and bottom-quark annihilation in the standard model and the MSSM*, *Comput. Phys. Commun.* **184** (2013) 1605 [arXiv:1212.3249] [INSPIRE].

[47] F. Borzumati, J.S. Lee and W.Y. Song, *Threshold corrections to* $m_b$ *and the* $b\bar{b} \to H_i^0$ *production in CP-violating SUSY scenarios*, *Phys. Lett.* **B 595** (2004) 347 [hep-ph/0401024] [INSPIRE].

JHEP05(2016)093